

Bifunctional Fluorocarbon Electrode Additive Lowers the Salt Dependence of Aqueous Electrolytes

Binghang Liu, Jintao Ma, Jingnan Feng, Ting Lin, and Liumin Suo*

The solid electrolyte interphase (SEI) plays a crucial role in extending the life of aqueous batteries. The traditional anion-derived SEI formation in aqueous electrolytes highly depends on high-concentrated organic fluorinating salts, resulting in low forming efficiency and long-term consumption. In response, this study proposes a bifunctional fluorocarbon electrode additive (BFEA) that enables electrochemical pre-reduction instead of TFSI anion to form the LiF-rich SEI and in situ produce conductive graphite inside the anode before the lithiation. The BFEA lowers the salt dependence of aqueous electrolytes, enabling the inorganic LiCl electrolyte to work first, but also successfully achieves a high SEI formation efficiency in the relatively low 10 m LiTFSI without mass transfer concerns, suppressing the parasitic hydrogen evolution from 11.24 to 4.35 nmol min⁻¹. Besides, BFEA strengthens the intrinsic superiority of Li storage reaction by lowering battery polarization resulting from the in situ production of graphite, promoting charge transfer of electrode kinetics. Compared with the control group, the demonstrated Ah-level pouch cell employing BFEA exhibits better cycle stability above 300 cycles with higher capacity retention of 78.2% and the lower decay of the round-trip efficiency ($\Delta_{\text{RTE}} = 2\%$), benefiting for maintaining the high efficiency and reducing heat accumulation in large-scale electric energy storage.

1. Introduction

Aqueous Li-ion batteries (ALIBs) are considered promising large-scale energy storage technology due to their nonflammability and environmental-friendliness.^[1] However, their cycling life is restricted by the narrow electrochemical window of aqueous electrolytes, resulting in the inevitable hydrogen evolution reaction

(HER) at the anode.^[2] Although water stabilization varies with temperature and pH, it is hard to apply in the practical application of aqueous batteries.^[3] Therefore, we think the proposal to form SEI passivation to offer kinetic protection against HER is much more effective and feasible, which has been widely verified in previous works.

SEI was first proposed in 1983 for Li metal, successfully assisting Li⁺ stripping and plating on Li metal anode and intercalation/de-intercalation of graphite in the subsequent development.^[4] In the context of an aqueous Li-ion battery, the SEI was believed to be absent in the early stage because the decomposition product of solvent H₂O and commonly used inorganic salts like LiCl, Li₂SO₄, LiNO₃, and LiClO₄ cannot form a deposition layer.^[3,5] Until 2015, SEI was finally feasible in the superconcentrated “Water-in-salt” electrolyte (WISE), where the organic salt LiTFSI was introduced as the solid source of SEI component, facilitating the LiF-rich SEI formation.^[1c] It effectively pushes the potential of HER much lower than

the lower redox potential anode, making the high-voltage aqueous batteries possible.

However, such conventional anion-derived SEI formation highly depends on expensive organic fluorine salts,^[6] such as LiTFSI,^[1c] LiOTf,^[7] LiBETI,^[8] and superhigh concentration,^[9] bringing out some inherent flaws as follows: 1) Anion-derived SEI formation does not have priority over the water decomposition since the hydrate cation is much closer to the polarized anode interface and the anions are repulsed by negatively charged electrode.^[10] The competition between HER and TFSI⁻ reduction causes a low SEI formation efficiency, consuming a longer time to form an effective SEI.^[3,5b,10b,e] 2) Anion-derived SEI suffers from dissolution and decomposition in the presence of free water, especially in moderate concentration WISE (10–15 m) compared to superconcentrated WISE (21 m).^[5b,10c,11] 3) The significantly increased salt concentration near the interface caused by water decomposition leads to salt deposition, which renders the SEI dynamic and not stable.^[12] Therefore, aqueous batteries need to explore a new way to make SEI formation and eliminate the dependence on salt to achieve a robust and energetic SEI in the early stages of cycling.

In addition, aqueous batteries face another common issue: the construction of SEI tends to increase battery polarization

B. Liu, J. Ma, J. Feng, T. Lin, L. Suo
Beijing National Laboratory for Condensed Matter Physics
Institute of Physics
Chinese Academy of Science
Beijing 100190, China
E-mail: suoliumin@iphy.ac.cn

B. Liu, J. Ma, J. Feng, L. Suo
Center of Materials Science and Optoelectronics Engineering
University of Chinese Academy of Science
Beijing 100190, China
L. Suo
Yangtze River Delta Physics Research Center Co. Ltd
Liyang 213300, China

The ORCID identification number(s) for the author(s) of this article can be found under <https://doi.org/10.1002/adma.202413573>

DOI: 10.1002/adma.202413573

and decrease round-trip efficiency. In large-scale energy storage, which is the most promising application for aqueous batteries, low round-trip efficiency can lead to significant heat buildup in battery packs, posing safety risks for MWh scale systems. To address the drawbacks of anion-derived SEI and polarization from SEI, in this work, we proposed a bifunctional fluorocarbon electrode additive (BFEA) that would be electrochemical pre-reduced instead of anion to form the LiF-rich SEI with high formation efficiency and priority without mass transfer concern and competition with anode lithiation or HER, suppressing side reactions and prolonging battery life. The byproduct amorphous carbon and graphite improve the conductive network, lower battery polarization, and strength the intrinsic superiority of Li storage reaction in the competition with HER. To sum up, BFEA greatly reduces the aqueous electrolyte's dual dependence on salt with expensive organic anion and superhigh concentration. It enables rapid and efficient SEI construction while simultaneously reducing battery polarization, which is highly beneficial for large-scale energy storage applications of aqueous batteries.

2. Results and Discussion

2.1. Design Salt-Independent SEI with High Formation Priority

First of all, we'll take the LMO//TiO₂ battery as an example to discuss in detail the issues associated with anion-derived SEI and present our design strategies to address these challenges.

Figure 1A shows the anode potential continuously decreases during the charging process. When the anode potential is greater than 2.2 V versus Li/Li⁺, it has not reached the lithiation potential of TiO₂. At this stage, LiTFSI in traditional WISE electrolytes decomposes to form the SEI. However, since LiTFSI reduction is a very slow process, its decomposition cannot provide sufficient electron transfer under constant current charging (>0.1C), causing the anode potential to drop rapidly to 2 V versus Li/Li⁺, where TiO₂ lithiation provides enough electron transfer. The core reason lies in the repulsion of anions by negative polarized anode, and the large size of TFSI⁻ further exacerbates the limitations of its mass transfer in electrolyte. This results in insufficient SEI formation in traditional WISE electrolytes before TiO₂ lithiation, even if high concentrations increase the decomposition potential of LiTFSI. The reduction of anion then has to compete with both anode lithiation and HER, further resulting in a very slow SEI formation efficiency that leads to significant lithium loss during the early cycles of the battery.

To address the issues of low SEI formation efficiency and competition between SEI and other reactions, the first step is to tackle the mass transfer problem. Therefore, we opted to design an electrode additive. Unlike electrolyte-based additives, electrode additives can be evenly mixed within the electrode and are not constrained by electrolyte mass transfer, ensuring their reaction speed. Additionally, the additive's electrochemical reduction potential should be much higher than the anode lithiation and HER, ensuring that SEI formation takes priority. Since LiF is widely recognized as an effective SEI component, we focused on finding an electrode additive with a high reduction potential that can form LiF.

Fluorocarbon (CF_x) perfectly meets these requirements as BFEA. It is already widely verified as a primary battery cathode

material.^[13] With a high reduction potential at ≈2.4 V versus Li/Li⁺, it can be quickly reduced during charging at the anode, forming LiF-rich SEI. Once BFEA is fully reduced and a complete LiF SEI is formed, the anode potential will drop to 2 V versus Li/Li⁺, where TiO₂ begins to be lithiated (**Figure 1A**). At this stage, HER will be suppressed significantly, because HER requires both electronic and ionic conduction and every active site where HER can occur is also where BFEA can undergo reduction earlier. The uniform mixing of BFEA ensures that the LiF SEI film it forms suppresses the HER of the electrode comprehensively, which is an additional advantage of electrode additive. With the help of the LiF SEI layer, TiO₂ lithiation becomes more favorable than HER, which allows for a clearer distinction of its lithiation peak in **Figure 1B** from HER peak and results in a smaller HER current than the control group. **Figure 1C** summarizes the comparison of potentials for BFEA reduction, TiO₂ lithiation, and HER, in LiTFSI and LiCl solutions. The above results demonstrate that the electrode additive BFEA can preferentially form LiF SEI during the initial charging cycle and effectively suppress HER.

In addition to addressing the low SEI formation efficiency (issue 1) caused by anion repulsion of anode and liquid-phase mass transfer as an electrode additive, BFEA also solves the other two anion-derived SEI issues mentioned in the introduction. Second, compared with conventional electrolyte-derived SEI, the amount of our BFEA is adjustable to control the amount of SEI formed and subsequently manage its dissolution (toward issue 2). Third, BFEA has a higher reduction potential than HER, which enables robust LiF-rich SEI to form first to avoid competition with HER, thereby ensuring that salt dissolution and deposition during water decomposition do not interfere with SEI formation (toward issue 3).

Additionally, there are various types of fluorocarbons. To address the battery polarization issue associated with SEI, we chose graphite fluoride as the BFEA, as research indicates it can more effectively reduce electrode resistivity compared to other fluorocarbons.^[14] The second function of the bifunctional BFEA in reducing battery polarization will be discussed in detail in the following sections.

A series of electrochemical experiments and characterization were carried out to verify the mechanism of BFEA to form LiF SEI. As shown in **Figure 2A**, the reduction of BFEA begins at 2.4 V versus Li/Li⁺, significantly earlier than TiO₂ lithiation at ≈2 V versus Li/Li⁺, ensuring the LiF formation does not compete with TiO₂ lithiation and HER. Similar results are reflected in the dQ/dV curve of the full cell in **Figure 2B**. The plateau corresponding to BFEA appears ≈1.85 V, much earlier than the charging plateau of ≈2.2 V for the LMO-TiO₂ redox couple.

After confirming the reduction potential of BFEA, the reduction products were analyzed. To verify the source of LiF, 20 m LiCl was selected as the electrolyte to ensure that the fluorine source was solely from BFEA. The XRD spectra in **Figure 2C** indicate the presence of LiF products in the CF_x electrode after charging, confirming its reduction mechanism. LMO-TiO₂ full cell using 20 m LiCl electrolyte was also fabricated to analyze whether the BFEA can construct a durable SEI layer in an aqueous electrolyte with an inorganic salt. The BFEA reaction occurs at the site where both electron and ion are available, and HER also tends to happen. However, the higher potential of BFEA guarantees that the active sites for HER will be preemptively covered by LiF, improving

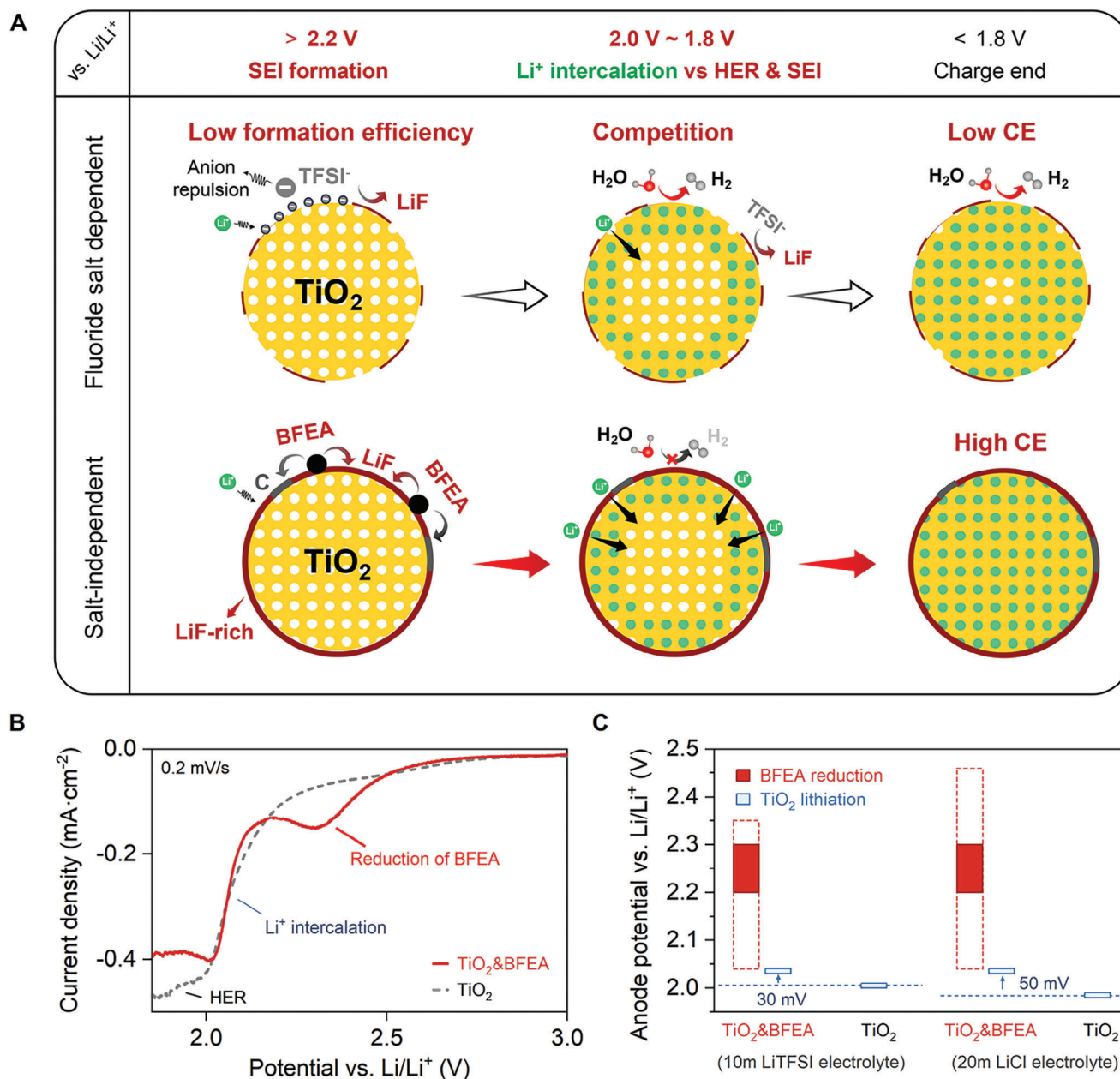


Figure 1. Mechanism of BFEA additive for SEI formation. A) The comparison between BFEA and WISE-dependent SEI formation. B) Cyclic voltammogram (CV) of the TiO_2 and TiO_2 &BFEA working electrode from 3 to 1.5 V versus Li/Li^+ , obtained at a scan rate of 0.02 mV s^{-1} in 20 m LiTFSI. C) Comparison of reaction potential of BFEA and TiO_2 . The data is derived from Figures 2A and 4A.

effectiveness. Among all the reaction sites across the conductive network, the three-phase sites of active material, conductive network, and electrolyte are our primary concerns, considering that the HER occurs the most. As shown in Figure 2D, LiF was densely coated on the surface of TiO_2 particles, providing excellent protection. The only area on the TiO_2 particle not covered by LiF shows significant accumulation of amorphous carbon, the contact point of the carbon conducting network with TiO_2 . It suggests that LiF-rich SEI covers the most reactive three-phase interface of TiO_2 , carbon conducting network, and electrolyte. Although BFEA has a micron-sized parti-

cle diameter, its reaction mechanism allows it to form nanoscale LiF to cover TiO_2 , consistent with previous studies.^[13e,15] The XPS spectra of cycled electrodes similarly demonstrate that BFEA can form a LiF SEI layer on active material even in non-fluorinated salt electrolytes such as 20 m LiCl, as shown in Figure 2F.

In summary, we have confirmed through various characterizations that BFEA can form a LiF-rich SEI layer on the active spots of the anode during battery charging, regardless of the type of electrolyte salt used. This LiF-rich SEI layer forms preferentially before anode lithiation and HER, offering a significantly higher

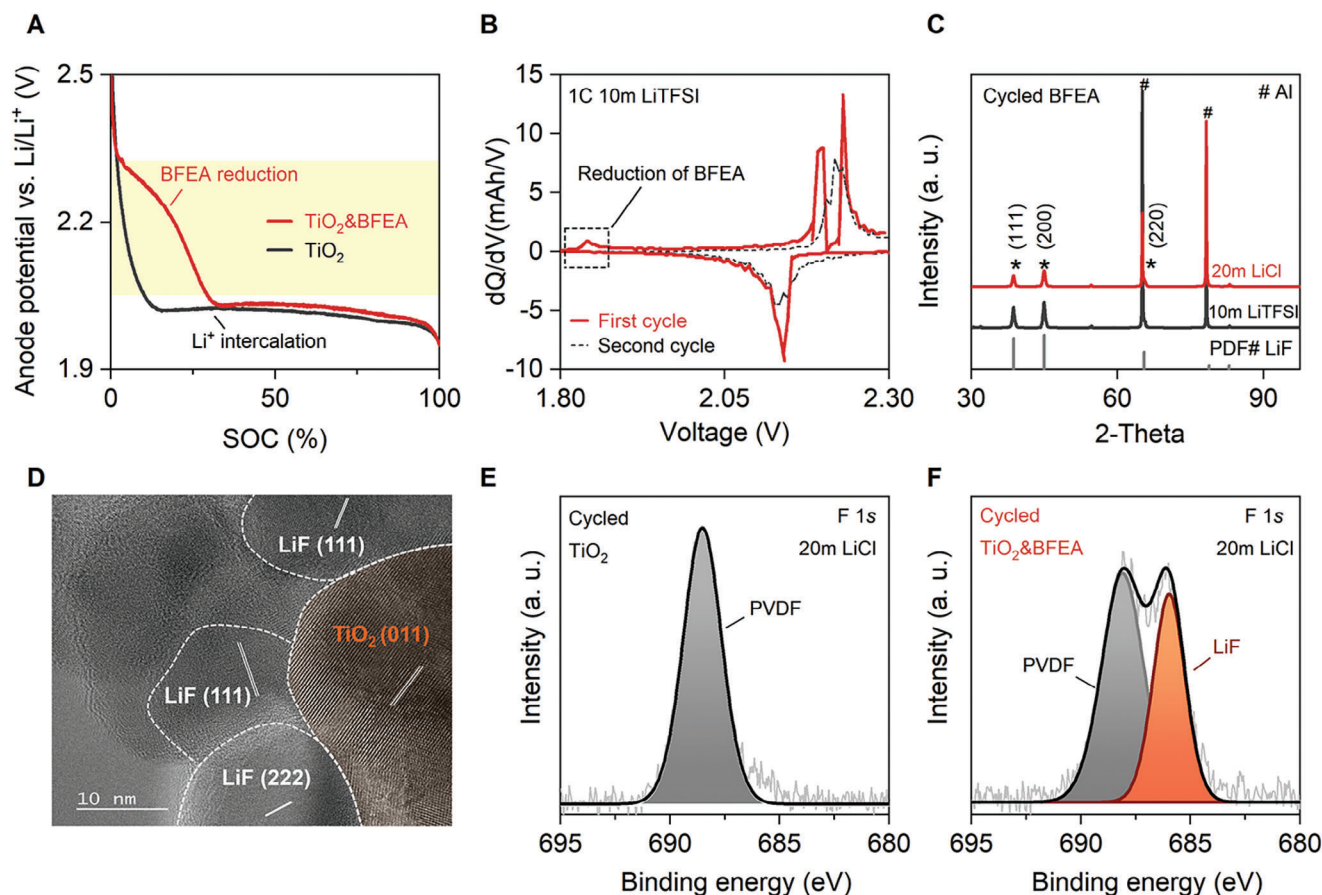


Figure 2. Clarify the SEI component from BFEA. A) BFEA reduction potential and TiO_2 lithiation potential comparison in 10 m LiTFSI. TiO_2 and TiO_2 &3%BFEA anodes are working electrodes with LMO as the counter electrode and Ag/AgCl as the reference electrode in the Swagelok cell. B) The dQ/dV plot of the first and second charge–discharge of LMO// TiO_2 &3%BFEA cell with 10 m LiTFSI. C) The XRD patterns of cycled CF_x anode in 10 m LiTFSI and 20 m LiCl, respectively. D) The TEM image of cycled TiO_2 &3%BFEA anode in 20 m LiCl. E, F) The X-ray photoelectron spectroscopy (XPS) spectrum of TiO_2 and TiO_2 &3%BFEA electrodes cycled in 20 m LiCl.

formation efficiency than the SEI formation via LiTFSI decomposition in WISE electrolytes.

2.2. Demonstrate the Function 1 of BEFA on HER Inhibition

The reduction of BFEA produces two products, LiF and carbon, each offering distinct benefits to the battery. This section focuses on the effect of LiF in suppressing side reactions such as HER and self-discharge, while the discussion on carbon is deferred to the next section. To quantify the suppression of HER by the BFEA, DEMS was used for in situ analysis of the hydrogen evolution rate in the full cell. As shown in **Figure 3B,C**, the cell with BFEA has a significantly lower hydrogen evolution rate than the control group in each of the first 5 cycles. The total hydrogen evolution in the control group during the first five cycles was 164.7% of that in the BFEA-added battery, demonstrating the highly effective passivation effect of BFEA. Notably, the hydrogen evolution rate continuously decreases with cycling (**Figure 3D**) due to the gradual formation of the SEI from the decomposition of LiTFSI in WISE. However, the hydrogen evolution rate decreases rapidly in the BFEA-added battery (BFEA: 50%, control group: 33%),

demonstrating that BFEA can synergize with LiTFSI to form a more robust SEI layer.

Additionally, the surface reactivity of the cycled electrodes was tested using SECM. The TiO_2 covered by SEI makes it difficult for indicator Fe^{3+} to get electrons on its surface for reduction, resulting in decreased feedback current at the probe. The average probe current of the regular TiO_2 electrode reached 0.74 pA, while the electrode with BFEA significantly reduced to 0.55 pA, and the current distribution was notably more uniform (**Figure 3E,F**). It indicates that the LiF-rich SEI formed from BFEA effectively covered the electrochemical reaction sites across the electrode, efficiently passivating the electrode and suppressing side reactions.

As conducting self-discharge testing of the batteries at 100% state of charge (SOC), the voltage maintaining duration of the LMO// TiO_2 &BFEA cell increased by 38.9% compared to the LMO// TiO_2 cell (**Figure 3G**). It indicates that the LiF-rich SEI effectively protects the lithiated TiO_2 , preventing reactions with water in the electrolyte and thereby reducing the battery's self-discharge.

To further examine the effect of the BFEA, electrolytes with nonfluorinated salt (LiCl) were used. Due to the reduction of BFEA forming a LiF-rich SEI and graphite as a byproduct

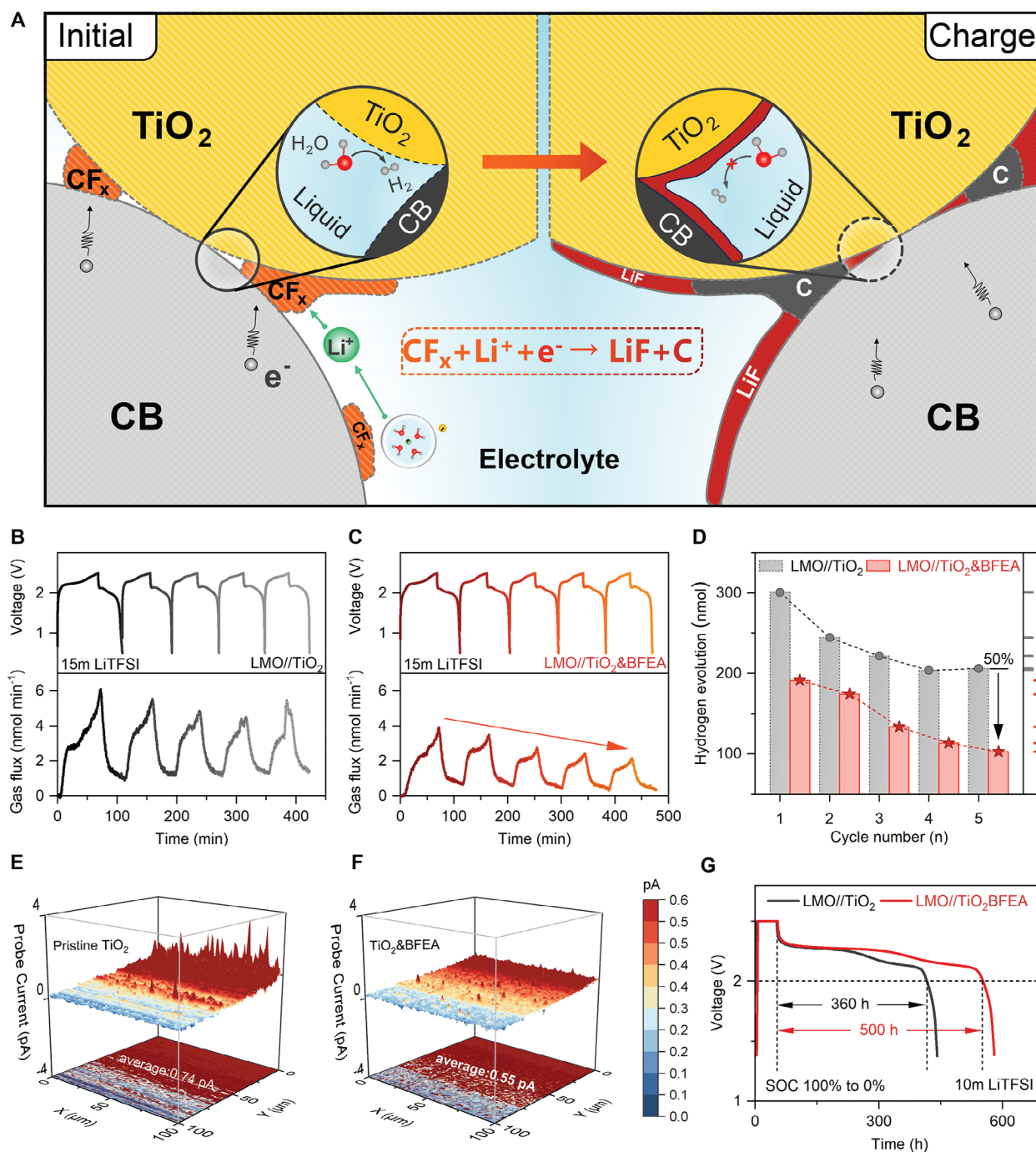


Figure 3. The inhibition effect of SEI on side reactions. A) The schematic of SEI formation by BFEA: $CF_x(s) + Li^+(aq) + e^- \rightarrow LiF(s) + C(s)$. B,C) The H₂ gas evolution in the initial five cycles of LMO//TiO₂ cell and LMO//TiO₂ & 3% BFEA cell with 15 m LiTFSI. D) The amount of H₂ generation in each of the first 5 cycles. E,F) The electrochemical activity of the TiO₂ and TiO₂ & 3%BFEA anode characterized through scanning electrochemical microscope (SECM). G) The self-discharge comparison at 100% SOC between LMO//TiO₂ cell and LMO//TiO₂ & 3%BFEA cell with 15 m LiTFSI.

reducing battery polarization, the lithiation of the TiO₂ with BFEA is facilitated. This makes TiO₂ lithiation more competitive against HER, as **Figure 4A** shows that its lithiation potential increased by nearly 0.1 V. On the other hand, the control group cannot form SEI layer, making HER more dominant over the anode lithiation, resulting in a very low discharge specific capac-

ity (72.3 mAh g⁻¹), as shown in **Figure 4B**. With the addition of BFEA, the discharge-specific capacity increased to 108.2 mAh g⁻¹ in **Figure 4B**. The effect of the LiF-rich SEI from BFEA in 20 m LiCl electrolyte is also reflected in the higher coulombic efficiency in **Figure 4C**. For another electrolyte with nonfluorinated salt, the 32 m KCH₃COO + 8 m LiCH₃COO electrolyte as reported by

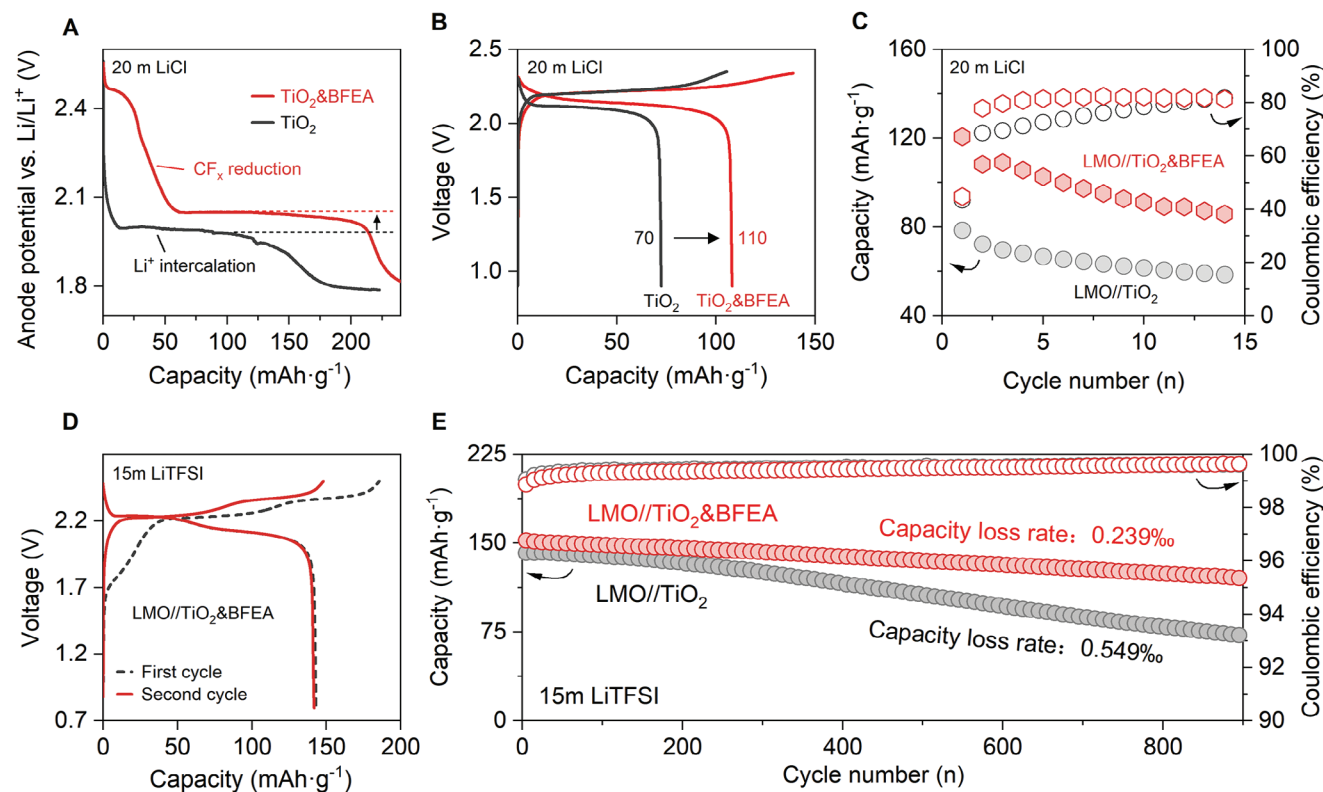


Figure 4. Cycling performance of ALIBs with BFEA additives with nonfluorinated/fluorinated salts. A) BFEA reduction potential and TiO_2 lithiation potential comparison in 20 m LiCl. TiO_2 and $\text{TiO}_2\&3\%\text{BFEA}$ anodes are working electrodes with LMO as the counter electrode and Ag/AgCl as the reference electrode in the Swagelok cell. B) The second cycle charge–discharge profiles of LMO/TiO_2 and $\text{LMO}/\text{TiO}_2\&3\%\text{BFEA}$ cell with 20 m LiCl. C) The cycling performances and coulombic efficiency of $\text{LMO}/\text{TiO}_2\&3\%\text{BFEA}$ cell and LMO/TiO_2 cell with 20 m LiCl at 1C. D) The first and second charge–discharge profiles of $\text{LMO}/\text{TiO}_2\&3\%\text{BFEA}$ cell with 15 m LiTFSI. E) The cycling performance and coulombic efficiency of the LMO/TiO_2 and $\text{LMO}/\text{TiO}_2\&3\%\text{BFEA}$ with 15 m LiTFSI at 1C. The mass ratio of LMO/TiO_2 is 2, and the specific capacity is calculated based on the TiO_2 anode.

Lukatskaya et al.,^[6] the cell with the addition of BFEA can achieve stable cycling for 50 cycles with excellent coulombic efficiency in Figure S18 (Supporting Information). The above results indicate that introducing BFEA provides an additional SEI construction method, which is highly versatile and can be adapted to various aqueous electrolytes.

However, purely inorganic electrolytes face more significant challenges regarding their electrochemical window. Solely relying on the kinetic regulation of SEI is still insufficient for practical applications in current systems. Therefore, we chose to use BFEA additives in the LiTFSI solutions to enhance its performance and application potential further. During the first charge process of the $\text{LMO}/\text{TiO}_2\&3\%\text{BFEA}$ full cell in 15 m LiTFSI, BFEA at anode gets reduced first, reflected as a plateau from 1.6 to 2.1 V in Figure 4D, corresponding to its specific capacity performance ($\approx 850 \text{ mAh g}^{-1}$) shown in Figures S14 and S15 (Supporting Information). Such a plateau disappears in the second cycle, indicating the full reduction of BFEA and LiF-rich SEI construction during the first charging process. The optimal addition ratio of BFEA was studied in Note S4 (Supporting Information). Considering various factors, an addition of 3% was found to be the most beneficial for enhancing cycling stability. As shown in Figure 4E, the capacity loss per cycle of the battery with 3% BFEA decreases from 0.55% to 0.24%. It indicates that adding BFEA contributes to a more complete and effective SEI construction than relying

solely on the decomposition of LiTFSI to form the SEI. More cycling stability tests with LiTFSI solutions with different concentrations are shown in Figures S19 and S20 and Note S5 (Supporting Information). All tests have shown that properly adding BFEA helps improve the battery cycle life.

2.3. Verify the Function 2 of BFEA in Lowering Battery Polarization

Although SEI can suppress side reactions and extend battery life, the continuous formation of SEI during cycling typically leads to increasing battery polarization, a common issue associated with SEI construction.^[5b] Therefore, when evaluating the performance of BFEA, we paid particular attention to its impact on battery polarization.

Semi in situ EIS measurements were used to investigate the impact of the reduction of the BFEA on the battery polarization. Figure 5B,D exhibits the raw data, connected with lines and the fitted Nyquist plots are shown in Figure S12 (Supporting Information). As the electrochemical reduction of BFEA, both R_{SEI} and R_{ct} decrease significantly and then stabilize. Regarding R_{SEI} , the F atoms in BFEA possess strong ionic properties before charging. When Li^+ diffuses on the surface of TiO_2 , the F atoms attract Li^+ , resulting in substantial interfacial impedance.^[16] As

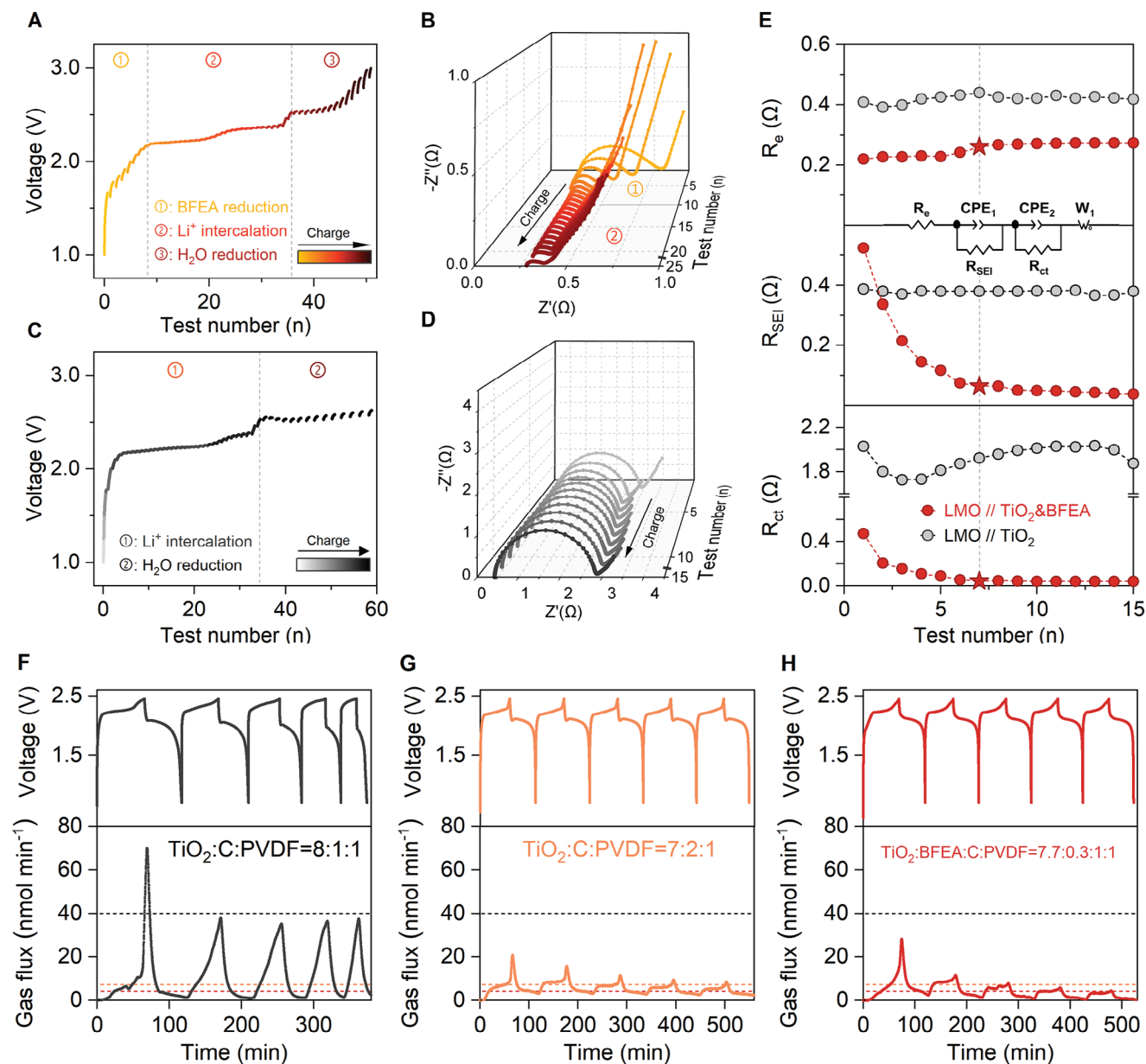


Figure 5. Influence of BFEA electrochemical reduction on battery polarization. A,C) The first charge profiles with EIS test after every 5 min-charge at constant current (0.3 C) of LMO//TiO₂&3%BFEA cell and LMO//TiO₂ cell in 15 m LiTFSI. B,D) The Nyquist plots of LMO//TiO₂&3%BFEA cell and LMO//TiO₂ cell. E) The comparison of the fitting results of the EIS spectra (Z' is the real part of the impedance, Z'' is the imaginary part of the impedance, R_e is the electrolyte resistance, R_{SEI} is the SEI resistance, R_{ct} is the charge transfer resistance, CPE is the constant phase angle element, and W_1 is the infinite diffusion impedance). F,G,H) The H₂ gas evolution in the initial five cycles of LMO//TiO₂ cell (TiO₂:C: PVDF = 8:1:1), LMO//TiO₂ cell (TiO₂:C: PVDF = 7:2:1) and LMO//TiO₂ & BFEA cell (TiO₂: BFEA:C: PVDF = 7.7:0.3:1:1) with 10 m LiTFSI.

BFEA is reduced, the F atoms gradually combine with Li⁺ to form LiF, reducing the hindrance caused by the F atoms and diminishing their impact on Li⁺ diffusion. It manifests as a continuous decrease in interfacial impedance. Once the reduction of BFEA is complete and the SEI on the anode interface is essentially formed, the interfacial impedance remains constant.

As for R_{ct} , earlier studies have shown that the carbon formed by the reduction of BFEA resembles a hard carbon structure, containing both amorphous carbon and graphite,^[13e,17] which improves the overall conductive network of the electrode.^[13e,14,18]

Additionally, previous research indicates that the binary conductive agents combination of micron-sized graphite and nanoscale carbon black helps reduce battery polarization and enhance rate performance,^[19] which aligns with our experimental results. Additionally, this reaction involves volume expansion,^[13e,20] which improves the contact between various components within the electrode and consequently lowers R_{ct} . In comparison, the impedance of the control group without BFEA remains relatively unchanged during the first charging process, indicating the minimal formation of SEI through LiTFSI and a small impact on the

battery. Besides, the LMO//TiO₂&BFEA full cell (10C 76.0 mAh g⁻¹) exhibits better rate performance than the LMO//TiO₂ full cell (10C 34.0 mAh g⁻¹) shown in Figure S13 (Supporting Information). Besides, the average output voltage at 10C increases 7.6%, and energy efficiency increases from 77.9% to 84.0% after adding BFEA, showing its excellent effect in improving conductive network and decreasing polarization.

Moreover, the HER overpotential of carbon (≈ 700 mV) is typically much higher than TiO₂ (≈ 400 mV),^[21] which suggests the carbon produced from BFEA may also suppress HER by increasing the side reaction's overpotential. To verify the HER inhibition effect of carbon, H₂ evolution rate were tested in full cells with 10 m LiTFSI as shown in Figure 5F,G,H. When the ratio of the anode components was adjusted from TiO₂: C: PVDF = 8:1:1 to 7: 2: 1, the increase of carbon significantly reduced the hydrogen evolution rate of the battery (from 37.5 to 8.6 nmol min⁻¹ the fifth-cycle peak), supporting the aforementioned conclusion. The effect of the BFEA was even more pronounced, with the experimental group having an electrode composition of TiO₂: BFEA: C: PVDF = 7.7: 0.3: 1: 1 showing a lowest HER peak rate (4.4 nmol min⁻¹) in the fifth-cycle. The addition of just 3% BFEA outperformed the effect of adding 10% carbon black. This indicates that the LiF-rich SEI constructed by BFEA, along with the high hydrogen evolution overpotential of the formed carbon, is much more effective in suppressing side reactions in aqueous batteries. To sum up, after adding 3% BFEA, the five cycles average hydrogen evolution rate decreases significantly from 11.24 nmol min⁻¹ (8:1:1 control group) to 4.35 nmol min⁻¹. More experiments of HER rate in full batteries with different electrode composition are shown in Figure S9 (Supporting Information), making the conclusion more reliable. It is important to mention that this experiment reduced the active material ratio to compare the effectiveness of BFEA and carbon. To avoid reducing the energy density of the battery, in practical applications, the electrode ratio of TiO₂: BFEA: C: PVDF = 8: m: 1-m: 1 is used, more details in the Experimental Section.

2.4. Demonstrate the Effectiveness of BFEA in Ah Level Pouch Cell

Finally, we verified the battery performance in 0.5 Ah full batteries (54.3 Wh kg⁻¹). The primary cause of degradation in aqueous batteries is the HER issue during charging. Although “water-in-salt” electrolytes partially solve this problem by lowering the activity of H₂O and forming anion-derived SEI through LiTFSI, HER is inevitable because the lithiation potential of the TiO₂ anode is significantly lower than the thermodynamic potential for HER to achieve a higher energy density. HER competes with the lithiation of the anode and leads to irreversible lithium loss, which subsequently causes continuous capacity decay. Therefore, suppressing HER through kinetical methods is the most promising way, among which SEI regulation is most effective and convenient. As shown in Figure 6A, the coulombic efficiency and 300-cycle capacity retention of LMO//TiO₂&BFEA cells (99.68% and 78.2%) are significantly higher than LMO//TiO₂ cells (99.57% and 53.0%). As discussed in Figure 5B, the carbon generated by the BFEA enhances the conductivity network of the TiO₂ anode, resulting in reduced polarization. Therefore, the

LMO//TiO₂&BFEA cell achieves a higher average energy efficiency (89.5%) and average output voltage (2.09 V) compared to the control group (87.8% and 2.04 V).

Notably, after 300 cycles, the round-trip efficiency of the battery with BFEA decreased only 2%, compared to a 6% decrease in the control group. The progressively decreasing round-trip efficiency during cycling poses a significant challenge for large-scale energy storage, as the lost energy dissipates as heat, leading to serious safety risks in MWh-level battery modules. By improving the electrode's conductive network and reducing battery polarization, BFEA significantly enhances the stability of round-trip efficiency, effectively addressing this issue.

Additionally, we closely examined the trends in average discharge and charge voltages in Figure 6F, noticing an asymmetry. As cycling progresses, the average discharge voltage of the LMO//TiO₂ battery decreases nearly three times faster (124 mV over 300 cycles) than the average charge voltage increases (40 mV over 300 cycles). This phenomenon may be related to the lithiation mechanism of TiO₂ explained by the core-shell model.^[22] Studies indicate that lithiated TiO₂ exhibits significantly higher conductivity than pristine TiO₂.^[23] For nanoscale TiO₂, the characteristic time for lithium-ion diffusion into the particle's interior can reach the order of 10⁴ seconds, much slower than the 1C rate used in the cycling.^[22c] Consequently, during charging, the outer layer of TiO₂ particles is lithiated first, rapidly improving conductivity. Due to the slow inward diffusion of lithium ions, the outer shell of the TiO₂ particles remains lithiated, ensuring good overall conductivity and significantly reducing the impact of polarization. However, during discharge, the lithiated outer shell of TiO₂ delineates first, causing the conductivity of TiO₂ particles in contact with the conductive network to deteriorate rapidly, which amplifies the effects of polarization. The underlying reason is the difference in conductivity resulting from the distinct lithiation distribution in TiO₂ during the charging and discharging stages at the same level of lithiation, as detailed in Figure S21 (Supporting Information). After adding BFEA, the battery's conductive network improves, compensating for the decreased overall conductivity of TiO₂ during discharge. As a result, the average output voltage variation over 300 cycles is reduced to 54 mV, a 55% improvement in voltage stability.

3. Conclusion

In this work, we have proposed a bifunctional BFEA to construct a LiF-rich SEI layer and reduce the battery polarization through the reduction product carbon. BFEA has a high 2.4 V versus Li/Li⁺ reaction potential before TiO₂ lithiation, thereby restraining the HER and prolonging the life of ALIBs. 3% addition of BFEA decrease the average H₂ generation rate from 2.78 nmol min⁻¹ to 1.5 nmol min⁻¹ in 15 m LiTFSI. Moreover, BFEA helps construct the SEI layer in 20 m LiCl, making anode lithiation dominant over HER and achieving a much higher discharge capacity (108.2 mAh g⁻¹) than the control group (72.3 mAh g⁻¹). In the practical 0.5 Ah battery, the experimental group exhibits significantly enhanced cycle life (300 cycles retention from 53.0% to 78%), much higher round-trip efficiency, and more stable output voltage. The higher round-trip efficiency, output voltage, and the semi in situ EIS experiments verify its effect on decreasing battery polarization. Additionally, we observed the asymmetry in

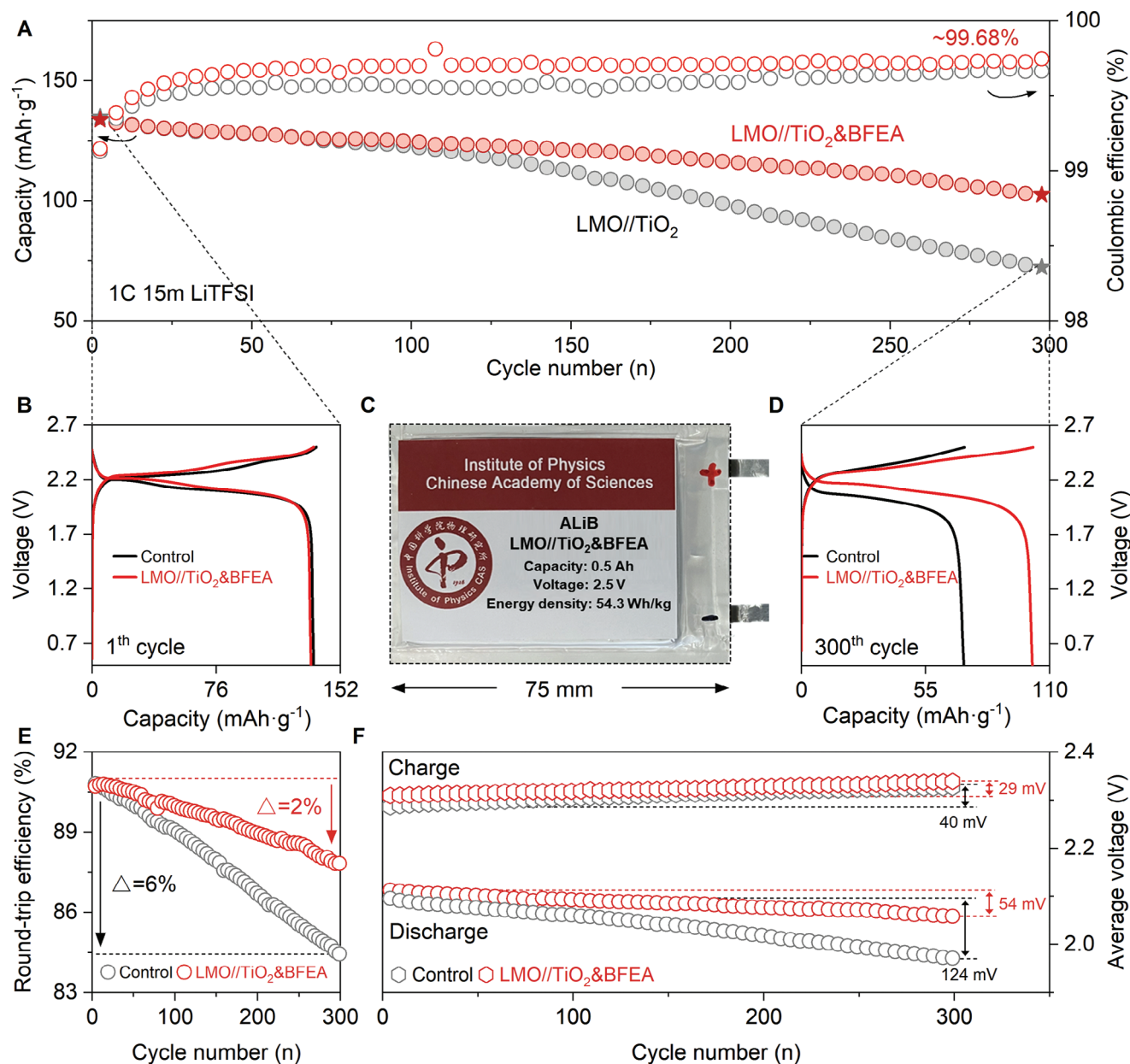


Figure 6. The practical performance of LMO//TiO₂ cell with BFEA in 0.5 Ah ALIBs. A) The comparison of the cycle stability and coulombic efficiency of LMO//TiO₂&3%BFEA cell and LMO//TiO₂ cell at 1C rate. B,D) The charge and discharge profiles of the 1st and 300th cycle. C) Practical photo of 0.5 Ah battery. E) The comparison of energy efficiency. F) The comparison of average charge and discharge voltage.

the variations of charge and discharge voltages during cycling in LMO//TiO₂ full cells and explained it using core-shell model of TiO₂ lithiation, further emphasizing the importance of the BFEA in improving electrode conductive network. More importantly, the method in this work for constructing SEI and controlling polarization is general and efficient, lowering the salt type and concentration dependence of ALIBs, requiring only the proper addition of BFEA during electrode preparation. This approach holds significant application value for large-scale adoption in ALIBs to prolong lifespan and control heat accumulation in battery module.

4. Experimental Section

Preparation of LiMn₂O₄ // TiO₂, LiMn₂O₄//TiO₂@BFEA Pouch Cell: Fluoride graphite (CF_x, Innochem Corporation), bis(trifluoromethane)sulfonimide lithium salt (LiTFSI, >98%, Shandong Hairong Corporation), Lithium chloride salt (LiCl, 99%, Innochem Corporation), potassium acetate salt (KCH₃COO, Innochem Corporation), lithium acetate salt (LiCH₃COO, Innochem Corporation), and Ultrapure water were commercially available. Fluorine-containing electrolytes (10 m LiTFSI, 15 m LiTFSI, 20 m LiTFSI) and inorganic electrolytes (20 m LiCl, 32 m KCH₃COO+8 m LiCH₃COO) were prepared at the desired molality (moles salt in kilogram solvent).

The LiMn_2O_4 cathode was prepared by mixing LiMn_2O_4 (MTI Corporation), carbon black (CB), and polyvinylidene fluoride (PVDF) at a weight ratio of 8:1:1 in N-methyl pyrrolidinone (NMP) in an SK-300SII CE mixing machine (SHASHIN KAGAKU Co., Ltd.) for 60 min at a speed of 2000 rpm to produce a black slurry. The slurry was spread uniformly on a clean Al or Ti foil and then dried at 80 °C for 2 h.

The TiO_2 anode was prepared by mixing the same CB, PVDF at a weight ratio of 8:1:1 and the same NMP as the solvent. The TiO_2 &BFEA anode was prepared by mixing fluorinated graphite (CF_x , $x \approx 0.9$, Innochem Corporation), CB, PVDF at several weight ratios of 80-m:m:10:10 in Figure S9 and Figures S9, S16, and S17 (Supporting Information) and 80:m:10:m:10 in other experiments. Both the TiO_2 anode and TiO_2 &BFEA anode were used the same process as the LiMn_2O_4 cathode and spread on the Al or Ti foil.

All pouch cells were assembled using polypropylene (PP) membrane as the separator, and Al plastic film as packaging. Small pouch cells (capacity ≤ 10 mAh) were assembled with unilaterally coated LiMn_2O_4 cathode (area: 3 cm \times 3.5 cm, thickness: ≈ 100 μm , and mass loading: ≈ 6 mg cm^{-2}), unilaterally coated TiO_2 or TiO_2 &BFEA anode (area: 3 cm \times 3.5 cm, thickness: ≈ 50 μm , and mass loading: ≈ 3 mg cm^{-2}) and PP separator (area: 3.5 cm \times 4 cm) and 300 μL electrolyte. The 0.5 Ah pouch cells were assembled with eight layers of double-sided coated LiMn_2O_4 cathode (area: 4.5 cm \times 5.8 cm and mass loading: ≈ 20 mg cm^{-2}), seven layers of double-sided coated TiO_2 or TiO_2 &BFEA anode (area: 4.3 cm \times 5.6 cm and mass loading: ≈ 12 mg cm^{-2}) and PP separator (width: 6 cm).

Electrochemical Measurements: The cyclic voltammogram (CV) curves were recorded on a CHI660E electrochemical workstation with a three-electrode system, TiO_2 or TiO_2 &BFEA anode as working electrode, LMO as the counter electrode and Ag/AgCl as the reference electrode with scanning rates of 0.2 mV s^{-1} between potentials of 1.5 and 3.0 V versus Li/Li⁺. The Swagelok cells were assembled with the same three-electrode system, TiO_2 or TiO_2 &BFEA anode as working electrode, LMO as the counter electrode, and Ag/AgCl as the reference electrode. Both the Swagelok cells and pouch cells were tested between 0.5 and 2.5 V at constant current (1C) using a multichannel battery test system (Land CT3001A).

The in situ differential electrochemical mass spectrometry (DEMS) was conducted using a commercial mass spectrometer (Hiden, Beijing) coupled with assembled cells. Before testing, the cells were ventilated for 2 h with ultrahigh-purity Ar to eliminate impurity gas. The Ar carrier gas flow was 1 mL min^{-1} . Meanwhile, the Swagelok cells were tested between 0.9 and 2.5 V at constant current (1 C) using a multichannel battery test system (Land CT3001A). The hydrogen evolution rate for each battery has been normalized based on the mass of the anode active material (mg).

The scanning electrochemical microscopy (SECM) on cycled TiO_2 or TiO_2 &BFEA anode was done using a CHI900D electrochemical workstation. The main body of the four-electrode open cell was made of polytetrafluoroethylene (PTFE). The PTFE cell was filled with the prepared electrolyte, and one of the working electrodes (TiO_2 or TiO_2 &BFEA substrate) was placed at the bottom, with the other working electrode (25 μm Pt microelectrode) sealed in glass as the SECM tip; Ag/AgCl was used as a reference electrode, and another Pt electrode served as a counter electrode. The electrode surface tilt was corrected before all measurements. The approach curves were recorded with a step size of 1 μm in the z-axis and 1 μm when the tip current or impedance change was shorter than 10%. An area scan was performed after the tip was positioned near the surface. Images with an area of 100 μm \times 100 μm and 625 points were taken using a wide step size of 4 μm along the x-axis and a height step size of 4 μm along the y-axis. Data were recorded by moving the tip to (x, y) = (0, 0) initially, sweeping along the x-axis at a step size of 100 μm for the first line scan, and then moving back to (x, y) = (0, 4) for the second line scan and so on. The TiO_2 or TiO_2 &BFEA anode as the substrate was from the cycled pouch cell, and the electrolyte used for SECM was 21 m LiTFSI containing 4 mM potassium ferricyanide ($\text{K}_3[\text{Fe}(\text{CN})_6]$, 99.5%, Innochem Corporation), which was used as redox mediator.

The semi in situ electrochemical impedance spectroscopy (EIS) measurements on pouch cells were taken using Autolab301 (Metrohm Autolab, Switzerland) electrochemical workstation. The pouch cell contains LMO positive electrode, TiO_2 or TiO_2 &BFEA anode, PP separator, and

10 m LiTFSI electrolytes were charged to 3 V at constant current (0.3 C). After every 5 min charging interval, it would be paused, and the EIS test was immediately conducted. The frequency ranged from 0.1 Hz to 1 MHz, and the Nyquist plots from the EIS measurements were fitted with the most appropriate circuit model using the Zview software.

Characterization: Scanning electron microscopy (SEM) images of cycled TiO_2 and TiO_2 &BFEA anode morphologies were taken using a Hitachi S-4800 field emission scanning electron microscope operated at 10 kV. X-ray diffractometer (XRD) patterns of cycled CF_x anode were taken using a Bruker D8 X-ray diffractometer ($\text{Cu-K}\alpha$, $\lambda = 1.5406$ Å, $2\theta = 10^\circ \sim 80^\circ$). High-resolution transmission electron microscopy (HRTEM) images of the morphologies of cycled TiO_2 &BFEA anode were taken using a spherical aberration-corrected transmission electron microscope JEOL ARM-200F at 200 kV. Before the testing above, the electrodes were soaked in alcohol for 30 min and washed three times to eliminate any residual lithium salts. An ESCALAB 250 Xi ThermoFisher performed the XPS analysis with Mg/Al K α radiation. All the binding energies were referenced to the C 1s line at 284.8 eV.

Supporting Information

Supporting Information is available from the Wiley Online Library or from the author.

Acknowledgements

B.L. and J.M. contributed equally to this work. This work was supported by the National Key Research and Development Program of China (2022YFB2404500), the National Natural Science Foundation of China (U22B20124), the CAS Youth Interdisciplinary Team, and the Center for Clean Energy.

Conflict of Interest

L.S., B.L., and J.M. are co-inventors for a patent of the electrode SEI additive CF_x in aqueous Li-ion battery, filed by Yangtze River Delta Physics Research Center and Institute of Physics, Chinese Academy of Science.

Data Availability Statement

The data that support the findings of this study are available from the corresponding author upon reasonable request.

Keywords

aqueous Li ion battery, battery polarization reduction, bifunctional electrode additive, fluorocarbon, SEI construction

Received: September 10, 2024

Revised: October 9, 2024

Published online:

- [1] a) W. Li, J. R. Dahn, D. S. Wainwright, *Science* **1994**, 264, 1115; b) Y. Wang, J. Yi, Y. Xia, *Adv. Energy Mater.* **2012**, 2, 830; c) L. Suo, O. Borodin, T. Gao, M. Olguin, J. Ho, X. Fan, C. Luo, C. Wang, K. Xu, *Science* **2015**, 350, 938; d) B. Liu, J. Yue, T. Lv, S. Wang, A. Zhou, X. Xiong, L. Suo, *ACS Appl. Energy Mater.* **2021**, 4, 4928; e) J. Yue, L. Suo, *Energy Fuels* **2021**, 35, 9228; f) B. Liu, T. Lv, A. Zhou, X. Zhu, Z. Lin, T. Lin, L. Suo, *Nat. Commun.* **2024**, 15, 2922.

- [2] a) D. Chao, W. Zhou, F. Xie, C. Ye, H. Li, M. Jaroniec, S.-Z. Qiao, *Sci. Adv.* **2020**, 6, eaba4098; b) H. Zhang, X. Liu, H. Li, I. Hasa, S. Passerini, *Angew. Chem., Int. Ed.* **2021**, 60, 598; c) Y. Liang, Y. Yao, *Nat. Rev. Mater.* **2023**, 8, 109.
- [3] Y. Sui, X. Ji, *Angew. Chem., Int. Ed.* **2024**, 63, e202312585.
- [4] E. Peled, *Lithium Batteries* **1983**, 43.
- [5] a) A. von Wald Cresce, K. Xu, *Carbon Energy* **2021**, 3, 721; b) L. Suo, D. Oh, Y. Lin, Z. Zhuo, O. Borodin, T. Gao, F. Wang, A. Kushima, Z. Wang, H.-C. Kim, *J. Am. Chem. Soc.* **2017**, 139, 18670; c) X. Geng, X. Hou, X. He, H. J. Fan, *Adv. Energy Mater.* **2024**, 14, 2304094.
- [6] M. R. Lukatskaya, J. I. Feldblyum, D. G. Mackanic, F. Lissel, D. L. Michels, Y. Cui, Z. Bao, *Energy Environ. Sci.* **2018**, 11, 2876.
- [7] L. Suo, O. Borodin, W. Sun, X. Fan, C. Yang, F. Wang, T. Gao, Z. Ma, M. Schroeder, A. von Cresce, *Angew. Chem.* **2016**, 128, 7252.
- [8] Y. Yamada, K. Usui, K. Sodeyama, S. Ko, Y. Tateyama, A. Yamada, *Nat. Energy* **2016**, 1, 16129.
- [9] J. Yue, J. Zhang, Y. Tong, M. Chen, L. Liu, L. Jiang, T. Lv, Y.-s. Hu, H. Li, X. Huang, *Nat. Chem.* **2021**, 13, 1061.
- [10] a) F. Wang, O. Borodin, M. S. Ding, M. Gobet, J. Vatamanu, X. Fan, T. Gao, N. Eidson, Y. Liang, W. Sun, *Joule* **2018**, 2, 927; b) Y. Shang, S. Chen, N. Chen, Y. Li, J. Lai, Y. Ma, J. Chen, F. Wu, R. Chen, *Energy Environ. Sci.* **2022**, 15, 2653; c) X. Hou, R. Wang, X. He, T. P. Pollard, X. Ju, L. Du, E. Paillard, H. Frielinghaus, L. C. Barnsley, O. Borodin, *Angew. Chem., Int. Ed.* **2021**, 60, 22812; d) X. Hou, T. P. Pollard, W. Zhao, X. He, X. Ju, J. Wang, L. Du, E. Paillard, H. Lin, K. Xu, *Small* **2022**, 18, 2104986; e) C. Yang, J. Chen, T. Qing, X. Fan, W. Sun, A. von Cresce, M. S. Ding, O. Borodin, J. Vatamanu, M. A. Schroeder, *Joule* **2017**, 1, 122.
- [11] a) Y. Shen, B. Liu, X. Liu, J. Liu, J. Ding, C. Zhong, W. Hu, *Energy Storage Mater.* **2021**, 34, 461; b) L. Droguet, G. M. Hobold, M. F. Lagadec, R. Guo, C. Lethien, M. Hallot, O. Fontaine, J.-M. Tarascon, B. M. Gallant, A. Grimaud, *ACS Energy Lett.* **2021**, 6, 2575; c) L. Droguet, A. Grimaud, O. Fontaine, J. M. Tarascon, *Adv. Energy Mater.* **2020**, 10, 2002440; d) D. Liu, Q. Yu, S. Liu, K. Qian, S. Wang, W. Sun, X.-Q. Yang, F. Kang, B. Li, *J. Phys. Chem. C* **2019**, 123, 12797; e) S. Ko, Y. Yamada, A. Yamada, *ACS Appl. Mater. Interfaces* **2019**, 11, 45554.
- [12] R. Bouchal, Z. Li, C. Bongu, S. L. e. Vot, R. Berthelot, B. Rotenberg, F. Favier, S. A. Freunberger, M. Salanne, O. Fontaine, *Angew. Chem.* **2020**, 132, 16047.
- [13] a) Z. Luo, X. Wang, D. Chen, Q. Chang, S. Xie, Z. Ma, W. Lei, J. Pan, Y. Pan, J. Huang, *ACS Appl. Mater. Interfaces* **2021**, 13, 18809; b) P. F. Fulvio, S. S. Brown, J. Adcock, R. T. Mayes, B. Guo, X.-G. Sun, S. M. Mahurin, G. M. Veith, S. Dai, *Chem. Mater.* **2011**, 23, 4420; c) C. Peng, Y. Li, F. Yao, H. Fu, R. Zhou, Y. Feng, W. Feng, *Carbon* **2019**, 153, 783; d) G. Zhong, H. Chen, X. Huang, H. Yue, C. Lu, *Front. Chem.* **2018**, 6, 50; e) B. Sayahpour, H. Hirsh, S. Bai, N. B. Schorr, T. N. Lambert, M. Mayer, W. Bao, D. Cheng, M. Zhang, K. Leung, *Adv. Energy Mater.* **2022**, 12, 2103196.
- [14] M. A. Reddy, B. Breitung, V. S. K. Chakravadhanula, M. Helen, R. Witte, C. Rongeat, C. Kübel, H. Hahn, M. Fichtner, *RSC Adv.* **2018**, 8, 36802.
- [15] N. Watanabe, T. Nakajima, R. Hagiwara, *J. Power Sources* **1987**, 20, 87.
- [16] J. Meng, Z. Xiao, L. Zhu, X. Zhang, X. Hong, Y. Jia, F. Liu, Q. Pang, *Matter* **2023**, 6, 1685.
- [17] N. Wang, Q. Liu, B. Sun, J. Gu, B. Yu, W. Zhang, D. Zhang, *Sci. Rep.* **2018**, 8, 9934.
- [18] a) B. Breitung, M. A. Reddy, V. S. K. Chakravadhanula, M. Engel, C. Kübel, A. K. Powell, H. Hahn, M. Fichtner, *Beilstein J. Nanotechnol.* **2013**, 4, 705; b) N. Sharma, M. Dubois, K. Guérin, V. Pischedda, S. Radescu, *Energy Technol.* **2021**, 9, 2000605; c) M. A. Reddy, B. Breitung, C. Wall, S. Trivedi, V. S. K. Chakravadhanula, M. Helen, M. Fichtner, *Energy Technol.* **2016**, 4, 201; d) M. A. Reddy, B. Breitung, V. S. K. Chakravadhanula, C. Wall, M. Engel, C. Kübel, A. K. Powell, H. Hahn, M. Fichtner, *Adv. Energy Mater.* **2013**, 3, 308; e) Y. Wang, Y. Zhang, W. Yang, S. S. Mao, W. Liu, R. Guo, Y. Luo, J. Xie, *Mater. Today Energy* **2018**, 10, 249.
- [19] a) S. Cheon, C. Kwon, D. Kim, S. Hong, H.-T. Kim, S. Kim, *Electrochim. Acta* **2000**, 46, 599; b) M. E. Spahr, D. Goers, A. Leone, S. Stallone, E. Grivei, *J. Power Sources* **2011**, 196, 3404; c) G. Yang, T. Takei, Y. Zhu, E. Iranmanesh, B. Liu, Z. Li, J. Wang, P. Hiralal, G. A. Amaratunga, O. Fontaine, *Electrochim. Acta* **2021**, 397, 139242; d) J. F. Baumgärtner, K. V. Kravchyk, M. V. Kovalenko, *Adv. Energy Mater.* **2024**, 2400499, <https://doi.org/10.1002/aenm.202400499>.
- [20] a) J. Read, E. Collins, B. Piekarski, S. Zhang, *J. Electrochem. Soc.* **2011**, 158, A504; b) C. Jiang, B. Wang, Z. Wu, J. Qiu, Z. Ding, J. Zou, S. Chen, P. Gao, X. Niu, L. Wang, *Nano Energy* **2020**, 70, 104552.
- [21] a) R. Li, B. Hu, T. Yu, Z. Shao, Y. Wang, S. Song, *Small Methods* **2021**, 5, 2100246; b) L. Nacamulli, E. Gileadi, *J. Appl. Electrochem.* **1983**, 13, 73; c) K. C. Ng, S. Zhang, C. Peng, G. Z. Chen, *J. Electrochem. Soc.* **2009**, 156, A846; d) S. Pérez-Rodríguez, E. Pastor, M. Lázaro, *Int. J. Hydrogen Energy* **2018**, 43, 7911; e) B. Ren, Q. Jin, Y. Li, Y. Li, H. Cui, C. Wang, *ACS Appl. Mater. Interfaces* **2020**, 12, 11607.
- [22] a) Q. Wei, X. Chang, D. Butts, R. DeBlock, K. Lan, J. Li, D. Chao, D.-L. Peng, B. Dunn, *Nat. Commun.* **2023**, 14, 7; b) M. Safari, M. Farkhondeh, M. Pritzker, M. Fowler, T. Han, S.-k. Chen, *Electrochim. Acta* **2014**, 115, 352; c) N. J. De Klerk, A. Vasileiadis, R. B. Smith, M. Z. Bazant, M. Wagemaker, *Phys. Rev. Mater.* **2017**, 1, 025404.
- [23] G. Cha, S. Mohajernia, N. T. Nguyen, A. Mazare, N. Denisov, I. Hwang, P. Schmuki, *Adv. Energy Mater.* **2020**, 10, 1903448.